Charged species profiles in oxygen plasma

S. V. Berezhnoj[a)] and C. B. Shin[b)]
Ajou University, Suwon, 442-749, Korea

U. Buddemeier and I. Kaganovich[c)]
Institute of Experimental Physics II, Ruhr-Universitaet Bochum, 44780 Bochum, Germany

(Received 24 March 2000; accepted for publication 7 June 2000)

The charged species profiles have been studied in oxygen plasma of asymmetrically driven capacitively coupled rf discharge. The electron (n_e), negative (n), and positive (p) ion densities have been measured by Langmuir probe in a wide range of pressures (3–30 Pa) and interelectrode distances (2–10 cm). At small powers ($n_e < 10^{15}\,\mathrm{m}^{-3}$) it was obtained that the electronegativity is high ($n/n_e \sim 10$) and the electron density profile is flat in plasma bulk. The negative ion density profile is nearly flat in the ion–ion core, where $n \gg n_e$, and falls off towards the plasma-sheath boundary with $n \approx 0$ with the spatial scale $\pi\sqrt{D_n/(2\gamma_d)}$, determined by the negative ion diffusion coefficient D_n and detachment frequency γ_d. As the pressure decreases, this spatial scale exceeds half of the interelectrode distance and the negative ion density profile tends to a parabolic one. The obtained spatial distributions of charged particles are compared with the results of self-consistent modeling by use of a fluid approach for ions, and kinetic equation for electrons. Numerical simulation results agree well with both theory predictions and measurement data. [S0003-6951(00)00532-5]

Processes in electronegative plasmas have attracted considerable attention due to interest to the problem of atmospheric electricity,[1] development of negative ion plasma sources,[2] and wide use of these plasmas in the plasma-aided materials processing industry.[3] It was shown theoretically that plasma transport of charged species in electronegative plasmas is nonlinear and very different from electropositive plasmas.[4,5] And it is expected that plasma stratifies into the ion–ion core ($n/n_e \gg 1$) and electropositive region ($n/n_e < 1$).[6] The indication of plasma stratification was observed in an experimental study of oxygen capacitively coupled plasmas.[7] However, the large asymmetry of the discharge in the Ref. 7 was a serious obstacle for interpretation of the experimental data.

This letter reports the systematic experimental and numerical study of charged species density profiles in oxygen electronegative plasmas in a wide range of pressures (3–30 Pa) and interelectrode distances (2–10 cm). For this purpose, the symmetrically rf ($\omega = 13.56\,\mathrm{MHz}$) driven capacitively coupled discharge was designed[8] with a variable gap. The large inner diameter (30 cm) compared to the interelectrode distance ($2L$) insured that plasma profiles can be described as a one-dimensional system. Electrodes were symmetrically driven to provide the symmetry of the plasma profile and the small oscillation of the plasma potential.[9] The charged species densities were measured by Langmuir probe with passive compensation up to 4ω Fourier harmonics. The electron energy distribution function (EDF) was obtained from the second derivative of the probe volt–ampere characteristic.[9] The electron density was found as an integral over the EDF. The negative ion density was measured by use of two methods: laser-induced photodetachment[10] and the ''double-peak''method similar to the electron density.[8] The positive ion density was obtained from ion saturation current by use of theory.[11]

The charged species density profiles were modeled by use of a fast modeling technique (FMT), which we successfully applied for modeling of electropositive plasmas.[12] FMT calculates discharge self-consistently including EDF, plasma bulk, and sheath region. We assumed a symmetric one-dimensional geometry and modeled only a half of the discharge.

Under the pressure range investigated, the ion mean-free path is small compared with L. Hence, ion fluid continuity equations may be used:

$$\frac{\partial n}{\partial t} - \frac{\partial}{\partial x}\left[D_n \frac{\partial n}{\partial x} + e\mu_n(E)En\right] = \nu_{\mathrm{att}} n_e - \gamma_d n - \beta_{ii} np, \tag{1a}$$

$$\frac{\partial p}{\partial t} - \frac{\partial}{\partial x}\left[D_p \frac{\partial p}{\partial x} - e\mu_p(E)Ep\right] = Z_{\mathrm{ioniz}} n_e - \beta_{ii} np. \tag{1b}$$

In the above equations, β_{ii} is the ion–ion recombination rate coefficient, and Z_{ioniz}, ν_{att}, and γ_d, are the ionization, attachment, and detachment frequencies, respectively. D_k and μ_k are the k-species diffusion coefficient and mobility.

The diffusion coefficients for O_2^+ and O^- adopted from Ref. 13 at 1 Pa are 0.65×10^4 and $0.92\times10^4\,\mathrm{cm}^2/\mathrm{s}$, respectively. The ion mobilities were taken from Ref. 13 as nonlinear functions of E/p.

Under the experimental conditions, as is shown in the Ref. 7, it is enough to consider the following charged species: positive ions $O_2{}^+$, negative ions O^-, and electrons. The densities of O_2^- and O_3^- reach only 10%–20% of the total negative density and can be omitted.[7]

The ionization and attachment frequencies in Eq. 1 are calculated by use of the EDF. We consider discharge at low

[a)]On leave from Physical Technical Department, St. Petersburg State Technical University, 195251, Russia;
electronic mail: berezhnoj@phtf.stu.neva.ru
[b)]Electronic mail: cbshin@madang.ajou.ac.kr
[c)]Current address: Plasma Physics Laboratory, Princeton University, NJ 08543; electronic mail: ikaganov@pppl.gov

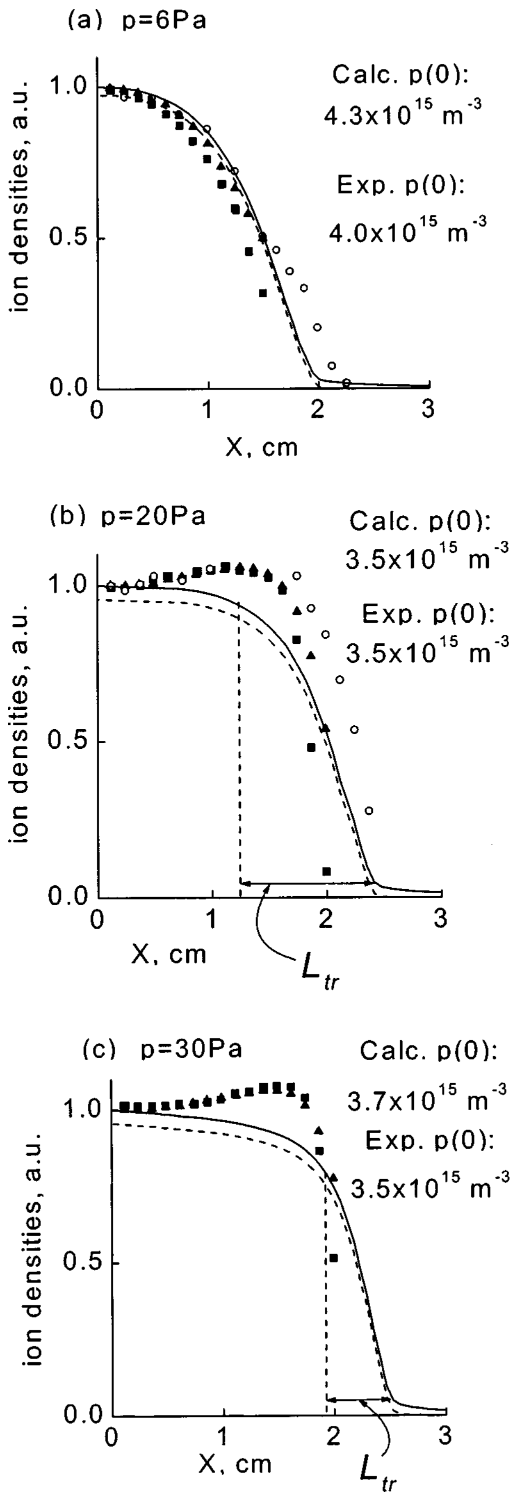

FIG. 1. (a), (b), and (c):. Experimentally and numerically obtained profiles of charged particles for $L=3$ cm, $\omega=13.56$ MHz, and $p=6$, 20, and 30 Pa ($j_o=0.31$, 0.35, and 0.35 mA/cm^2). Solid and dashed lines represent calculated densities of positive and negative ions, respectively. Symbols represent experimental data. Solid squares denote the negative ion density measured by the ''double-peak'' method, triangles denote the positive ion density measured by the ''saturation'' method, and hollow circles represent the negative ion density measured by the photodetachment method. $p(0)$ shown in the pictures are the densities of the positive ions at the discharge center.

powers, when the ion and electron densities are small ($n,p,10n_e \sim 10^{15}\,\mathrm{m}^{-3}$). Hence, ion–ion and electron–ion recombination can be neglected. The main source of the negative ion losses is detachment of electrons due to collisions of negative ions with the metastable molecules O_2^* in O_2 ($a^1\Delta_g$) state with the rate $3\times10^{-10}\,\mathrm{nn_m}$,[14] where n_m is the O_2 ($a^1\Delta_g$) density. n_m is to be obtained from the continuity equation

$$-\frac{\partial}{\partial x}\left(D_m\frac{\partial}{\partial x}n_m\right)=I_m, \qquad (2)$$

where D_m is the metastable diffusion coefficient (at 1 Pa it is 2.1 $10^4\,\mathrm{cm^2\,s^{-1}}$) and I_m is the rate of electron excitation of metastable molecules determined by use of the EDF. A boundary condition for Eq. (2) is of the form $[D_m\partial(n_m)/\partial x - sv_{th}n_m]|_{x=L}=0$, where v_{th} is the thermal velocity of metastable molecules and $s=10^{-3}$ is the coefficient of the deactivation of metastable molecules during collisions with the wall.[15]

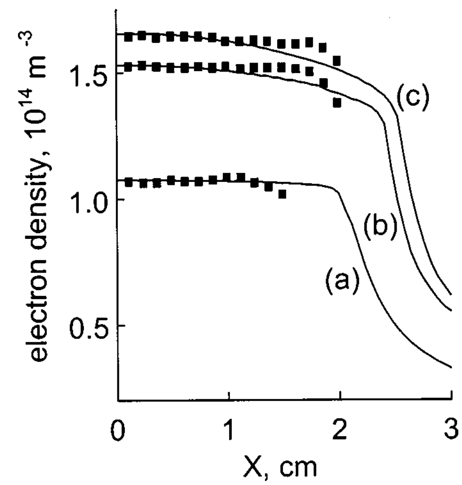

FIG. 2. Electron density for the same parameters as in Figs. 1(a), 1(b), and 1(c). The curves represent the calculated results. Symbols represent the electron density obtained by integrating the measured EDF.

In Fig. 1, the measured and calculated profiles of ion densities are presented jointly for $p=6, 20$, and 30 Pa; $L=3$ cm. For the same parameters, profiles of the electron density are shown in Fig. 2. Calculated fluxes of ions corresponding to the results in Fig. 1 are shown in Fig. 3.

The experimental and calculated values of the ion densities and sheath thickness agree well. Since we did not use any fitting parameters, the good agreement validates the plasma chemical model described above.

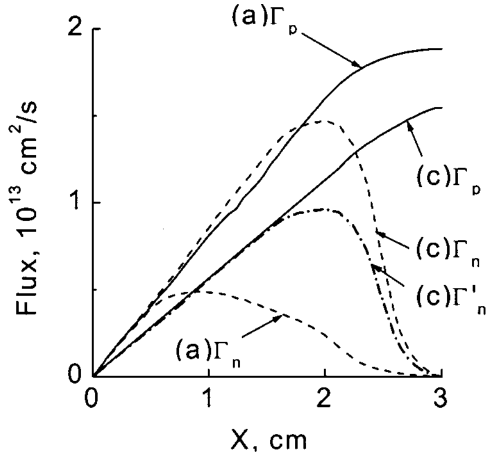

FIG. 3. Calculated ion fluxes for the same parameters as in Figs 1(a), and 1(c). Dashed lines represent the negative ion fluxes. The line marked as Γ_n' corresponds to the negative ion flux divided by $D_n/D_p\approx1.415$.

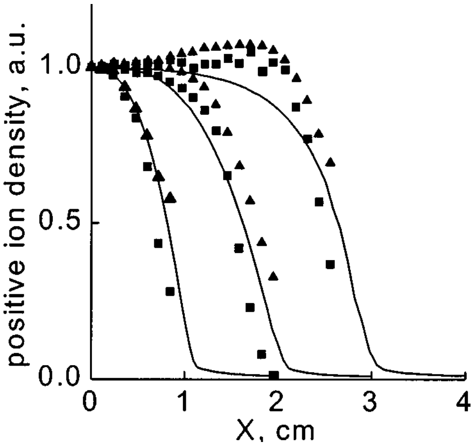

FIG. 4. Positive ion profiles are presented for $p=10$ Pa, $\omega=13.56$ MHz, $jo=0.35$ mA/cm^2, and $L=2, 3, 4$ cm. Squares denote the negative ion density measured by the ''double-peak'' method. Triangles denote the positive ion density measured by the ''saturation'' method. The experimentally and numerically obtained values of $p(0)$ are 3.9, 4.0, and 3.4×10^{15} and 4.31, 4.37, and 3.2×10^{15} cm^{-3} for $L=2$, 3, and 4 cm, respectively.

The shape of the ion density profile is close to the parabola at lower pressures ($p=6P$ a). As can be seen from Fig. 3, the negative ion flux is much smaller than the positive ion flux. Consequently, in this case negative ions are in Boltzmann equilibrium $eE=-T_i d \ln n/dx$, the electric field is small, and the electron density is flat. From ion continuity Eq. (1b), it follows that in ion–ion core ($n \gg n_e$) the ion ambipolar diffusion coefficient is $2D_i$ because the ion recombination is small. Equation (1b) gives the parabolic profile of the ion density.[6,16] As the pressure increases, the attachment rises and the negative ion flux becomes comparable to the positive ion flux. That indicates that the drift term becomes larger than the diffusion terms in the fluxes. Under this conditions, the assumption of the negative ions being in Boltzmann equilibrium is not valid. In this limiting case the assumption of equal ion fluxes (with factors $1/D_p$ and $1/D_n$) can be used[6,17] [see Fig. 3 ($p=30$ Pa) the negative ion flux divided by D_n/D_p versus the positive ion flux]. Equality of the fluxes results in the equality of the right-hand sides of Eq. (1):

$$(Z_{\text{ioniz}} D_n/D_p + \nu_{\text{att}}) n_e - \gamma_d n - (1 + D_n/D_p)\beta_{ii} n p = 0. \tag{3}$$

For not very high pressures and large gaps, it can be shown that the electron density profile still remains flat[6,17] (see Fig. 2). And from Eq. (3) it follows that the ion densities are also flat in the ion–ion core region [see Figs. 1(b) and 1(c)]. The width of the transition region from the plasma sheath boundary to the ion–ion core can be found as follows.[6] Summing up Eq. (1) with factors $1/D_p$ and $1/D_n$ and assuming the Einstein relation for the ratio of the ion diffusion coefficient and mobilities and the electron Boltzmann relation $eE = -T_e d \ln n_e/dx$, yields

$$-2\frac{d^2 n}{dx^2} - \frac{T_e}{T_i}\frac{d^2 n_e}{dx^2} = \left(\frac{Z_{\text{ioniz}}}{D_p} + \frac{\nu_{\text{att}}}{D_n}\right) n_e - \frac{\gamma_d}{D_n} n - \left(\frac{1}{D_n} + \frac{1}{D_p}\right)\beta_{ii} n p. \tag{4}$$

The profile of n_e is flat and the second term on the left-hand side of Eq. (4) can be neglected at low pressures.[6] For low-density plasmas, the ion–ion recombination is small compared with the detachment and the solution of Eq. (4) is

$$n = n^0\left[1 - \exp\left(\sqrt{\frac{\gamma_d}{2D_n}}(x - L_p)\right)\right], \tag{5}$$

where $n^0 = (D_n/\gamma_d)(Z_{\text{ioniz}}/D_p + \nu_{\text{att}}/D_n) n_e$ is the value of the negative ion density in the ion–ion core and L_p is the difference between L and the sheath thickness. Therefore, the width of the transition region from the plasma sheath boundary to the ion–ion core ($n = 0.957 n^0$) is $L_{\text{tr}} = e/\sqrt{\gamma_d/2D_n}$. Substituting values for the detachment frequency and the ion diffusion coefficient yields $L_{\text{tr}} = 0.30/p(Pa) \times \sqrt{n_e(10^{14} m^{-3})}$ m. It gives $L_{\text{tr}} = 5.0$, 2.6, 1.2, and 0.63 cm for $p = 6, 10, 20$, and 30 Pa, respectively. For $p=6$ and 10 Pa, $L_{\text{tr}} > L_p$ and it corresponds to the case when the discharge width is not enough for the formation of the flat ion–ion core. For $p=20$ and 30 Pa, $L_{\text{tr}} < L_p$ and the flat ion–ion core appears. In Fig. 4, the ion density profiles for different discharge gaps are depicted for $p=10$ Pa; $L=2$, 3, and 4 cm. It can be seen that if the gap width is extended beyond $L_{\text{tr}} = 2.6$ cm, the flat ion–ion core is formed. In the opposite case the parabolic profile is observed. The estimated values of L_{tr} are close to the width of the transition regions obtained in the experiment [see Figs. 1(b) 1(c) and 4].

The work of one of the authors (I.K.) was funded by the National Science Foundation, Grant No. CTS-9713262, and by the Alexander von Humboldt Foundation. One of the authors (U.B.) was supported by the Deutsche Forschungsgemeinschaft through the Sonderforschungsbereich 191. One of the authors (S.B.) was supported by KISTEP Program No. 99RI06-016, by INTAS Grant No. 96-0235, and by UTS Grant No. 378. The work of one of the authors (C.B.S.) was supported by KOSEF Grant No. 951-1107-018-2.

[1] W. Swider, *Ionospheric Modeling* (Birkhauser, Basel, 1988).
[2] M. Hopkins and K. Mellon, Phys. Rev. Lett. **67**, 449 (1991).
[3] M. A. Lieberman and A. J. Lichtenberg, *Principles of Plasma Discharges and Materials Processing* (Wiley, New York, 1994).
[4] I. D. Kaganovich and L. D. Tsendin, Plasma Phys. Rep. **19**, 645 (1993).
[5] I. Kaganovich, D. J. Economou, B. N. Ramamurthi, and V. Midha, Phys. Rev. Lett. **84**, 1918 (2000).
[6] L. D. Tsendin, Sov. Phys. Tech. Phys. **34**, 11 (1989).
[7] D. Vender, W. W. Stoffels, E. Stoffels, G. M. W. Kroesen, and F. G. de Hoog, Phys. Rev. E **51**, 2425 (1995).
[8] U. Buddemeier, Ph.D. thesis, Ruhr Universitaet (1997).
[9] V. Godyak and R. Piejak, Plasma Sources Sci. Technol. **1**, 36 (1992).
[10] M. Bacal, Plasma Sources Sci. Technol. **2**, 493 (1993).
[11] Yu. M. Kagan and V. I. Perel, Usp. Fiz. Nauk **81**, 1055 (1978).
[12] S. V. Berezhnoi, I. D. Kaganovich, and L. D. Tsendin, Plasma Sources Sci. Technol. **7**, 268 (1998).
[13] E. W. McDaniel and E. A. Mason, *The Mobility and Diffusion of Ions in Gases* (Wiley, New York, 1973).
[14] I. A. Kossyj, A. Yu. Kostinsky, A. A. Matveev, and V. P. Silakov, Plasma Sources Sci. Technol. **1**, 207 (1992).
[15] R. L. Sharpless and T. G. Slanger, J. Chem. Phys. **91**, 7947 (1989).
[16] A. J. Lichtenberg, V. Vahedi, M. A. Lieberman, and T. Ronglien, J. Appl. Phys. **75**, 2339 (1994).
[17] A. J. Lichtenberg, I. Kouznetsov, Y. T. Lee, M. A. Lieberman, I. D. Kaganovich, and L. D. Tsendin, Plasma Sources Sci. Technol. **6**, 437 (1997).